



Depth Dose According to Depth during Cone Beam Computed Tomography Acquisition and Dose Assessment in the Orbital Area Using a Three-Dimensional Printer

Min Ho Choi¹, Dong Yeon Lee¹, Yeong Rok Kang², Hyo Jin Kim²

¹Department of Radiological Science, Dong-Eui University, Busan, Korea; ²Dongnam Institute of Radiological & Medical Sciences, Busan, Korea

Original Research

Received January 17, 2024


Revision March 25, 2024

Accepted April 11, 2024

Corresponding author: Dong Yeon Lee

Department of Radiological Science,
Dong-Eui University, 176 Eomgwang-ro,
Busanjin-gu, Busan 47340, Korea
E-mail: gymnist@deu.ac.kr
 <https://orcid.org/0000-0002-9360-1897>

Co-corresponding author: Yeong Rok Kang

Dongnam Institute of Radiological &
Medical Sciences, 40 Jwadong-gil,
Jangan-eup, Gijang-gun, Busan 46033,
Korea
E-mail: yeongrok@dirams.re.kr
 <https://orcid.org/0000-0003-2981-6559>

This is an open-access article distributed under the terms of the Creative Commons Attribution License (<http://creativecommons.org/licenses/by-nc/4.0/>), which permits unrestricted use, distribution, and reproduction in any medium, provided the original work is properly cited.

Copyright © 2024 The Korean Association for Radiation Protection



ABSTRACT

Background: Cone beam computed tomography (CBCT) is essential for correcting and verifying patient position before radiation therapy. However, it poses additional radiation exposure during CBCT scans. Therefore, this study aimed to evaluate radiological safety for the human body through dose assessment for CBCT.

Materials and Methods: For CBCT dose assessment, the depth dose was evaluated using a cheese phantom, and the dose in the orbital area was evaluated using a human body phantom self-fabricated with a three-dimensional printer.

Results and Discussion: The evaluation of radiation doses revealed maximum doses of 14.14 mGy and minimum doses of 6.12 mGy for pelvic imaging conditions. For chest imaging conditions, the maximum doses were 4.82 mGy, and the minimum doses were 2.35 mGy. Head imaging conditions showed maximum doses of 1.46 mGy and minimum doses of 0.39 mGy. The eyeball doses using a human body phantom model averaged at 2.11 mGy on the left and 2.19 mGy on the right. The depth dose ranged between 0.39 mGy and 14.14 mGy, depending on the change in depth for each imaging mode, and the average dose in the orbit area using a human body phantom was 2.15 mGy.

Conclusion: Based on the experimental results, CBCT did not significantly affect the radiation dose. However, it is important to maintain a minimal radiation dose to optimize radiation protection following the as low as reasonable achievable principle.

Keywords: Depth Dose, Radiation Therapy, Cone Beam Computed Tomography, Dose Assessment

Introduction

Radiation therapy stands as a key cancer treatment method alongside surgery and chemotherapy. Additionally, the field of radiation therapy has continuously developed for decades because of the development of diagnostic imaging equipment, such as computed tomography (CT), magnetic resonance imaging, and positron emission tomography, along with the advancement in computer technology [1]. The advent of the multileaf collimator has enabled the implementation of intensity-modulated radiation therapy, minimizing radiation damage to normal tissues while concentrating the pre-

scription dose on the lesion, unlike conventional two-dimensional (2D) and three-dimensional (3D) conformal radiation therapies [2–4]. However, this precise radiation technique requires accurate patient positioning owing to the intricate delivery of varied radiation intensities. To address these issues, image-guided radiation therapy (IGRT) was adopted, which enhances treatment precision by capturing the patient's image just before treatment and comparing it with the reconstructed image from the treatment plan, which increases overall treatment accuracy [5]. Previously, beam's eye view imaging was utilized in IGRT, using the actual treatment beam to confirm the arrangement of the beam and target organs irradiated through the electronic portal imaging device to verify the treatment position. However, because beam's eye view uses megavoltage energy, which is treatment energy, it produces poor image quality and radiation exposure. Therefore, current therapeutic linear accelerators incorporate a diagnostic X-ray generator to obtain images suitable for identifying anatomical structures. The diagnostic X-ray generator mounted on the linear accelerator reduces unnecessary exposure by enabling the acquisition of both 2D (anterior-posterior [AP] and lateral [LAT]) and 3D (cone beam computed tomography [CBCT]) images. CBCT can pinpoint treatment positions by identifying normal and tumor tissues in three dimensions [6], making it crucial for precision treatment techniques involving complex-shaped target volumes and rapid changes in dose distribution [7, 8].

The acquisition of CBCT images leads to added radiation exposure, warranting consideration of stochastic effects and potential risks [9]. Moreover, delivering doses to both tumor and normal tissues might surpass the prescribed treatment plan, potentially impacting treatment efficacy.

Therefore, this study aimed to evaluate radiological safety by analyzing the radiation distribution in the human body and evaluating the radiation dose from CBCT imaging acquisition.

Materials and Methods

1. Experimental Equipment

1) Linear accelerator

The X-ray volumetric imager (XVI) attached to the linear accelerator (Elekta Versa HD) (Fig. 1) was used in the experiment. XVI can verify the patient's position by taking 2D, AP, and LAT images. However, limitations were encountered when correcting the patient's position during sophisticated

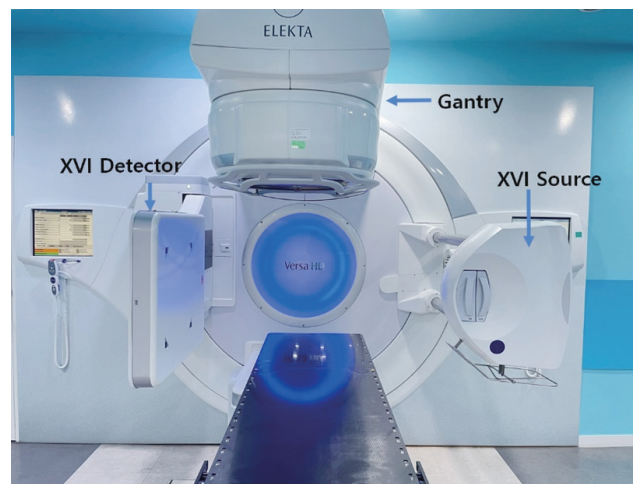


Fig. 1. A linear accelerator and an X-ray volumetric imager (XVI) system.

and precise radiation therapy using only the X, Y, and Z axes. Therefore, CBCT was developed to complement this. CBCT acquires images through a 360° gantry rotation, reconstructing them into 3D images that correct setup errors in the X, Y, and Z axes, as well as pitch, roll, and yaw directions, which is beneficial for treatment plans with sophisticated and precise dose distribution [10]. Additionally, its usage frequency is rapidly increasing owing to the advantage of checking the inside of the human body through black-and-white (grayscale) images [11].

2) Phantom

(1) Cheese phantom

The water phantom is the most basic phantom used in quality assurance for medical linear accelerator equipment. The water phantom measures various aspects, such as dose depth and beam flatness. The water phantom can conduct measurements with the gantry fixed in place. However, for this study, there were limitations to experimenting with the water phantom because the aim was to evaluate the dose received by the human body during CBCT imaging, where the gantry rotates. Therefore, the research team chose the cylindrical cheese phantom with a diameter of 30 cm and a length of 18 cm, as shown in Fig. 2. The cheese phantom is designed to allow the installation of dosimeters at specific depths and is composed of materials equivalent to water, making it suitable for evaluating human dose exposure.

Relative evaluation of the dose using a film in the center of the circle and absolute evaluation of the dose by inserting an ion chamber can be performed simultaneously. In addi-

tion, there are 20 plugs, including four solid water plugs and 16 tissue substitute plugs with an electron density of 0.29–4.59 g/cm³ for water on the other side. These are used in image calibration through the Hounsfield unit value of CT density [12, 13].

(2) Human body phantom

A human body phantom was fabricated using a 3D printer (Fig. 3) to investigate the effect on the actual human body. 3D modeling was performed by Materialize Mimics 21 software (Materialize) using a DICOM file that imaged the Rando phantom with Biograph mCT 64 (Siemens) to fabricate the phantom. J850 pro (Stratasys) was used as a 3D printer, and the polyjet printing method, which is a mixture of light curing and inkjet methods, was used. The head and neck were divided into 10 tomographic planes, with the ability to insert a glass dosimeter into the orbital area, corresponding to the fourth tomographic plane. In a study by Alssabbagh et al. [14], nine 3D printing materials were compared and analyzed with the mass attenuation coefficient of the human body to verify tissue reproduction, and the optimal 3D printing material was identified. Materials such as polycarbonate (PC), acrylonitrile butadiene styrene, thermoplastic polyurethane (TPU),

and polylactic acid (PLA) were compared and analyzed with the mass attenuation coefficient of human tissues such as the brain, breast, lens, kidney, and skin [14]. Table 1 shows the elements and densities of the 3D printing materials used in this study. Filament materials, composed of substances similar to the human body, encompass nine representative types. Based on existing literature, TPU material was employed for the eyes and skin, whereas PLA, the filament ma-



Fig. 3. A human body phantom fabricated using a three-dimensional printer. (A) Head and neck phantom divided into 10 layers. (B) Head and neck phantom with single-layer assembly.

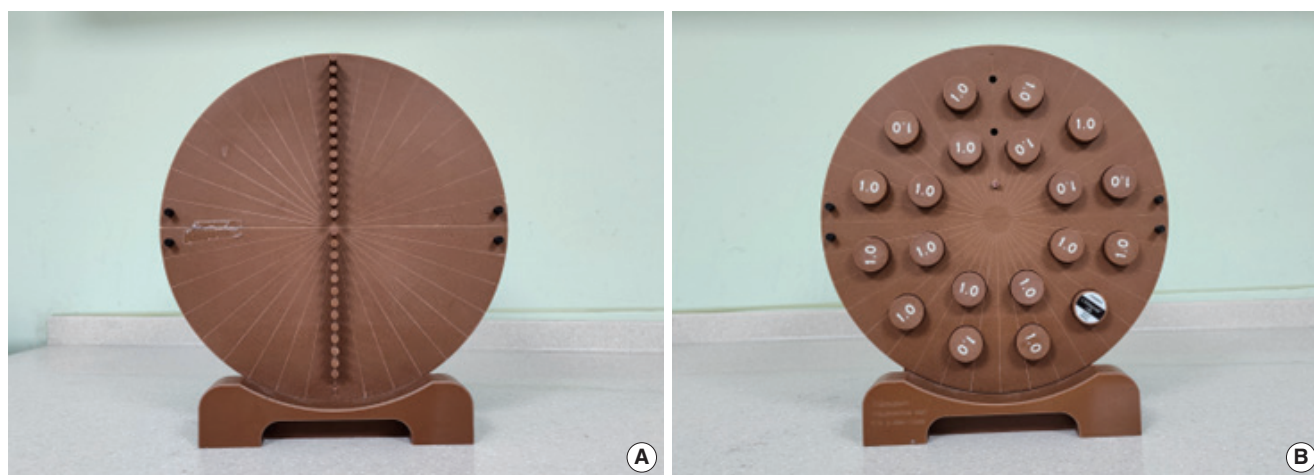


Fig. 2. (A) Front and (B) back of the cheese phantom.

Table 1. Elements and Density of 3D Printing Materials Used

Material	Elemental composition (%)									Density (g/cm ³)
	C	N	O	Al	Si	S	K	Ca	Ti	
PLA	54.76		44.99			0.13	0.12			1.25
TPU	66.63	8.98	24.13	0.06	0.10			0.09		1.10
PC	76.28		22.79			0.11			0.82	1.21

3D, three-dimensional; PLA, polylactic acid; TPU, thermoplastic polyurethane; PC, polycarbonate.

terial with the highest density, was selected for bones. However, given that PLA material has a density of approximately 0.4 g/cm^3 lower than that of bones, PC material with a density of approximately 0.2 g/cm^3 higher was used for the brain region to offset this disparity. The size of the phantom was derived from the Rando phantom, with dimensions set at a length of 28 cm and a depth of 19 cm for the cranial part.

3) Glass dosimeter

Fig. 4 shows the dosimeter used for measurement, which consists of a glass dosimeter (GD-352M; AGC Techno Glass) and a reader (FGD-1000SE; AGC Techno Glass). A glass dosimeter is effective for dose assessment in small fields because the handling and reading process is simple and the effective size is small [15]. Unlike a thermoluminescence dosimeter, it can be read repeatedly, has excellent device-to-device reproducibility, and has low energy dependence on photons. Therefore, it is widely used in dose assessment [16]. In this study, we selected a glass dosimeter capable of measuring radiation exposure from rotating sources and simultaneously measuring multiple dosimeters at different depths. The glass components of the glass dosimeter were calibrated using a ^{137}Cs standard radiation source. Prior to the experiment, the components underwent annealing by heating at $400 \text{ }^\circ\text{C}$ for 1 hour, followed by cooling, after which the initial values were measured. Subsequently, after preheating at $70 \text{ }^\circ\text{C}$ for 1 hour following the experiment, the dose values measured on the components were repeatedly measured 10 times to calculate the average value and standard deviation.

2. Experimental Method

1) Dose assessment according to depth change

First, we measured the radiation exposure index, computed tomography dose index (CTDI), which serves as a funda-

mental dose parameter in CT scans. We measured the CTDI values in the air under the pelvis, chest, and head imaging conditions. Additionally, we measured the CTDI weighted average of center and periphery dose (CTDI_w) values, considering both the central and peripheral regions. CTDI_w is defined by Equation (1).

$$\text{CTDI}_w = \frac{1}{3}\text{CTDI}_{\text{center}} + \frac{2}{3}\text{CTDI}_{\text{peripheral}} \quad (1)$$

During radiation therapy CBCT scans, the tumor's target position varies with the treatment area and patient. Furthermore, the positions and types of normal organs differ at each location. As point doses or CTDI represent the dose at a specific location or from a radiation source, assessing target tumor or normal organ doses based on position changes becomes limited. Therefore, we attempted to predict the absorbed dose resulting from the CBCT scan at various positions by assessing dose changes at different depths.

As shown in Fig. 5, glass dosimeters were inserted into holes created at 1 cm intervals from the surface to the center point of the cheese phantom, accompanied by the insertion of pencil-shaped solid water sticks. Subsequently, images were acquired. Dose measurement involved assigning numbers to the holes, with the one closest to the surface labeled as number 1 and the center as number 13 (Fig. 6). CBCT scans were performed using scan modes configured for body parts (head, chest, and pelvis) during routine clinical practice, as detailed in Table 2. Average doses were assessed by repeating measurements five times for each scan mode.

2) Dose assessment in the orbit area using the human body phantom

The orbit contains major visual organs in the human body, including the eyeball, optic nerve, iris, and retina, with the

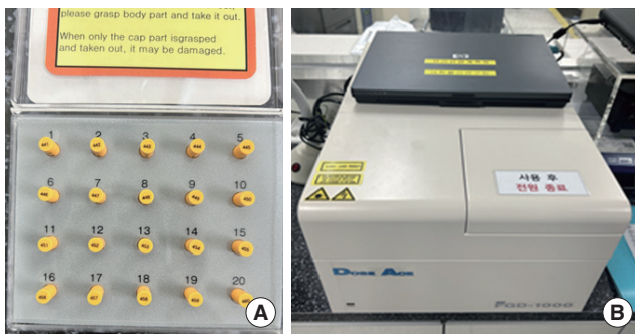


Fig. 4. A glass dosimeter and a reader. (A) A glass dosimeter. (B) A glass dosimeter reading equipment.

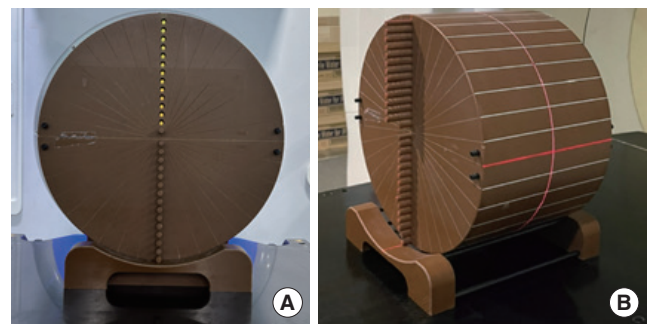


Fig. 5. (A) A photograph of glass dosimeters and (B) solid water sticks inserted.

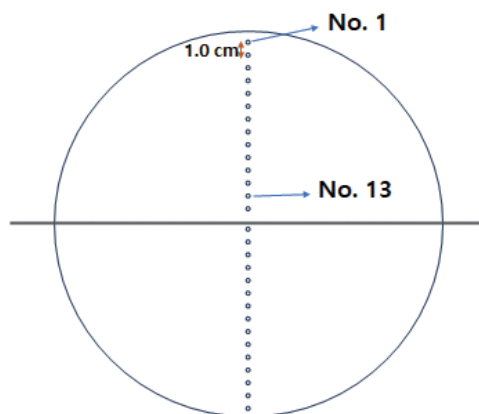


Fig. 6. Schematic diagram of cheese phantom.

Table 2. Scan Modes for Cheese Phantom

Body part	Scan mode
Head	100 kV, 10 mA 10 ms, F0 filter+S20 filter
Chest	120 kV, 20 mA 20 ms, F1 filter+M20 filter
Pelvis	120 kV, 40 mA 40 ms, F1 filter+L20 filter

lens being relatively more sensitive to radiation exposure than general skin tissue [17]. Therefore, the International Commission on Radiological Protection (ICRP) recently proposed a lowered value of approximately 7.5 times the lens dose equivalent limit recommended in ICRP 103 [18]. In light of continued reports on lens-related risks and their significance, underscoring the imperative for proper management, we assessed the dose to the orbital area, encompassing the lens, during CBCT acquisition utilizing the human body phantom.

CBCT scan was performed in the head scan mode among the modes previously set for depth dose assessment after inserting glass dosimeters into three positions in the left and right eyes of the orbital area located in the fourth single layer of the self-fabricated human body phantom (Fig. 7). Average doses were evaluated after repeated measurements three times by separating inserts for the left eye (eye 1, eye 2, and eye 3) and right eye (eye 1, eye 2, and eye 3).

Results

1. Measurement Results on Cheese Phantom According to Depth Changes

Table 3 presents the CTDI values obtained from the XVI source. In the air, the CTDI values were observed to be 49.6 mGy for the pelvis, 11.9 mGy for the chest, and 1.3 mGy for head conditions, respectively. Additionally, considering both central and peripheral doses, CTDI_w values were deter-

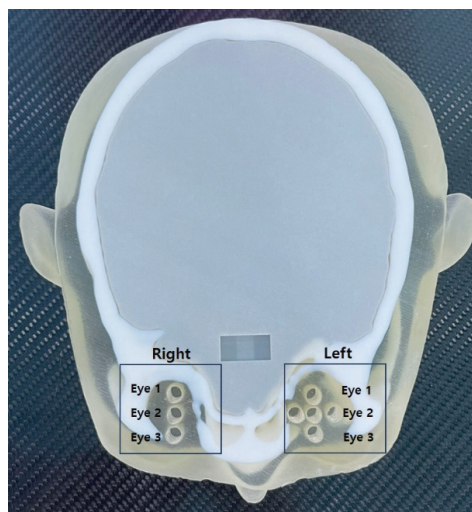


Fig. 7. Insertion positions of glass dosimeters into the human body phantom.

Table 3. Computed Tomography Dose Index by Scan Mode

CT dose index	Scan mode (mGy)		
	Pelvis	Chest	Head
CTDI _w	26.8	4.9	1.0
CTDI _{air}	49.6	11.9	1.3

CT, computed tomography; CTDI_w, computed tomography dose index weighted average of center and periphery; CTDI_{air}, computed tomography dose index free-in-air.

mined to be 26.8 mGy for the pelvis, 4.9 mGy for the chest, and 1.0 mGy for the head conditions, respectively.

Figs. 8–10 illustrate the experimental results of dose evaluation according to depth variation under pelvis, chest, and head imaging conditions. The Y-axis represents the absorbed dose, whereas the X-axis represents the glass dosimeters inserted into the cheese phantom. The measurement results of glass dosimeters from 1 to 13 are shown, with 1 being the closest to the surface and the numbers increasing towards the center.

Fig. 8 is a graph of average values measured using the cheese phantom according to the changes in depth under the pelvis scan mode. The highest measurement was 14.14 ± 0.32 mGy at point 1, closest to the surface. The lowest measurement was 6.12 ± 0.08 mGy at point 11 and 6.40 ± 0.17 mGy at point 13, the most central point.

Fig. 9 is a graph of average values measured using the cheese phantom according to the changes in depth under the chest scan mode. The highest measurement was 4.82 ± 0.15 mGy at point 1. The lowest was 2.35 ± 0.10 mGy at point 12 and 2.44 ± 0.12 mGy at point 13, the most central point.

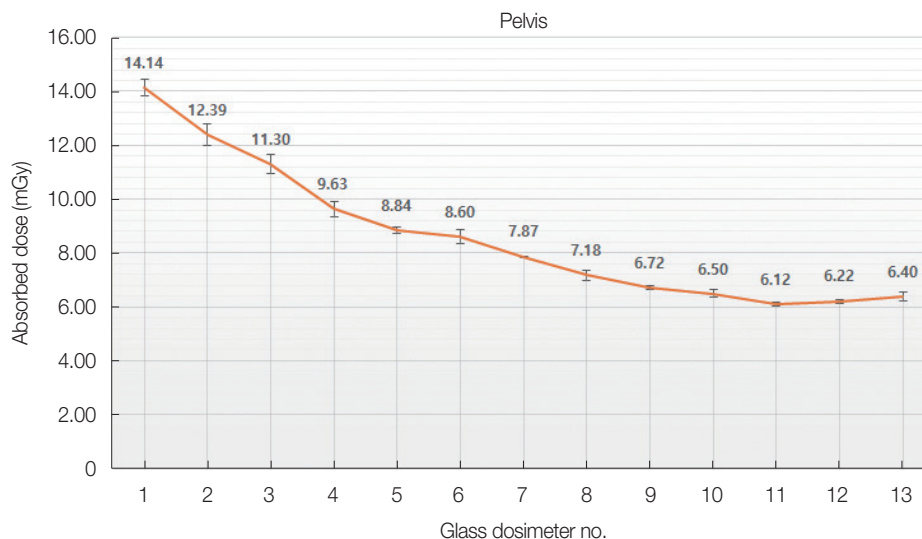


Fig. 8. Dosimetry results according to depth change (pelvis).

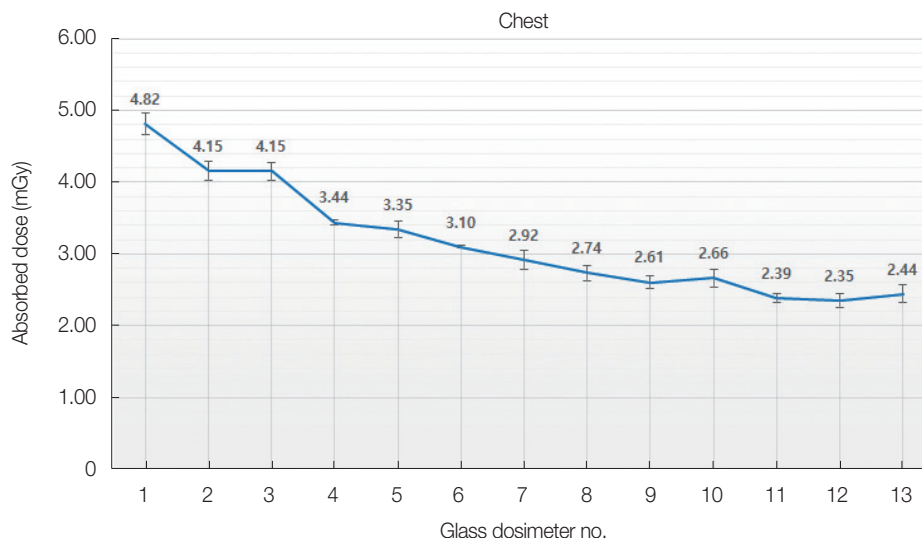


Fig. 9. Dosimetry results according to depth change (chest).

Fig. 10 is a graph of average values measured using the cheese phantom according to depth changes under the head scan mode. The highest measurement was 1.46 ± 0.00 mGy at point 1. The lowest measurement was 0.39 ± 0.01 mGy at point 12 and 0.41 ± 0.01 mGy at point 13, the most central point.

The means and standard deviations of the measured values under the three scan modes are listed in Table 4. The doses decreased under the three scan modes as the depth increased. The highest dose was measured under the pelvis scan mode. The standard deviations averaged 2.06% under the pelvis mode, 3.28% under the chest mode, and 3.03% under the head mode. The overall average was 2.79%.

2. Dosimetry Results on Human Body Phantom

Table 5 lists the dosimetry results of the orbital area using the human body phantom. Fig. 11 shows the dose for eye 1, eye 2, and eye 3 positions in the left and right eyes. The X-axis represents the positional variation from eye 1, the innermost part of the eyeball in the manufactured human body phantom, to eye 3, the outermost part where the lens is located. The Y-axis represents the absorbed dose. In the left eye, the average dose for eye 1 position was 2.08 ± 0.14 mGy, that for eye 2 was 2.06 ± 0.10 mGy, and that for eye 3 was 2.19 ± 0.15 mGy. In the right eye, the average dose for eye 1 was 2.13 ± 0.12 mGy, 2.14 ± 0.14 mGy for eye 2, and 2.29 ± 0.10 mGy for eye 3. The highest dose was measured at eye 3

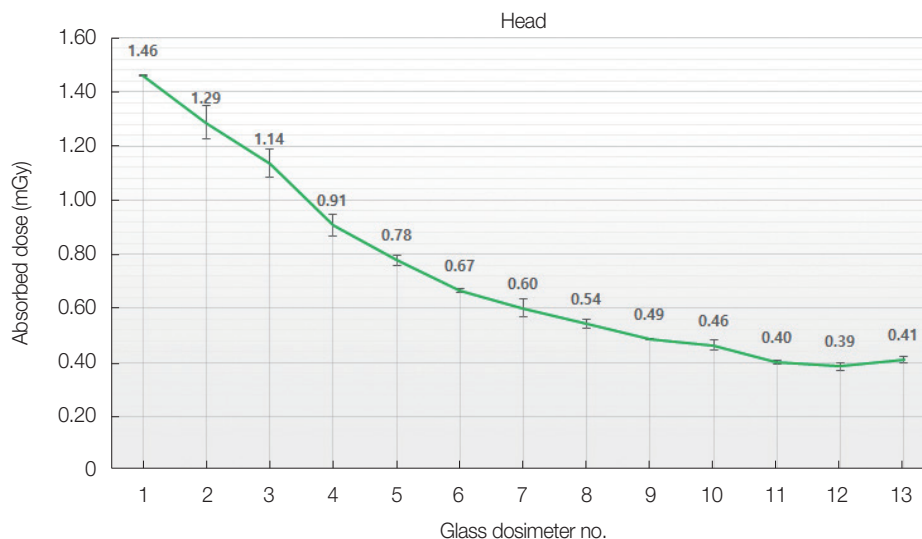


Fig. 10. Dosimetry results according to depth change (head).

Table 4. Means and Standard Deviations of Dosimetry According to Depth Changes

Glass no.	Scan mode (mGy)					
	Pelvis		Chest		Head	
	Mean	SD	Mean	SD	Mean	SD
1	14.14	0.32	4.82	0.15	1.46	0.00
2	12.39	0.42	4.15	0.13	1.29	0.06
3	11.30	0.37	4.15	0.13	1.14	0.05
4	9.63	0.27	3.44	0.04	0.91	0.04
5	8.84	0.11	3.35	0.12	0.78	0.02
6	8.60	0.25	3.10	0.02	0.67	0.01
7	7.87	0.02	2.92	0.13	0.60	0.03
8	7.18	0.18	2.74	0.10	0.54	0.02
9	6.72	0.05	2.61	0.09	0.49	0.00
10	6.50	0.14	2.66	0.12	0.46	0.02
11	6.12	0.08	2.39	0.07	0.40	0.01
12	6.22	0.07	2.35	0.10	0.39	0.01
13	6.40	0.17	2.44	0.12	0.41	0.01

SD, standard deviation.

position, close to both the left and right eye surfaces.

Fig. 12 shows the average doses to the left and right eyes in the orbital area. The average dose to the left eye (eye 1, eye 2, and eye 3) was 2.11 ± 0.11 mGy, and the average dose to the right eye (eye 1, eye 2, and eye 3) was 2.19 ± 0.11 mGy.

Discussion

This study analyzed the dose distribution based on position during CBCT acquisition, which is widely used in clinical practice, by evaluating the dose according to depth. In addition, we aimed to ascertain its potential application in

Table 5. Dosimetry Results in the Orbital Area Using a Human Body Phantom (mGy)

	1 st		2 nd		3 rd	
	Left	Right	Left	Right	Left	Right
Eye 1	2.15	2.07	2.18	2.27	1.92	2.05
Eye 2	2.03	2.06	2.17	2.30	1.98	2.06
Eye 3	2.04	2.18	2.34	2.37	2.19	2.31
Average	2.07	2.11	2.23	2.31	2.03	2.14

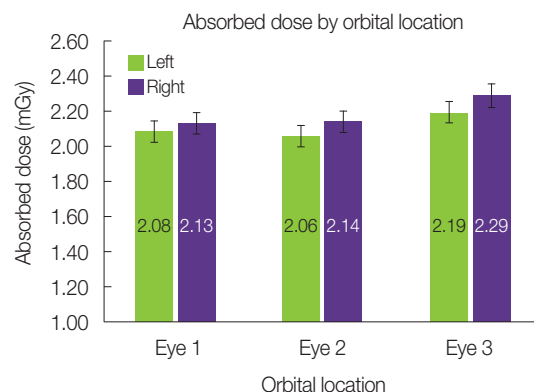


Fig. 11. Average dose by position of the left and right eyes in the orbital area.

clinical settings through dose assessment of the orbital area using a human body phantom created with a 3D printer.

Analysis revealed that additional doses were generated from CBCT scans performed during IGRT. In an experiment using the cheese phantom, high radiation exposure was observed in the sequence of pelvis, chest, and head. This is believed to be due to the relatively high tube voltage, tube cur-

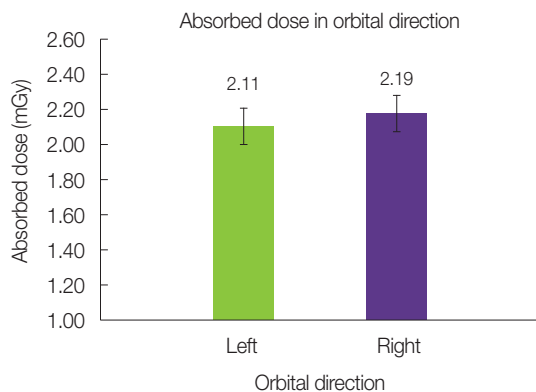


Fig. 12. Average doses to the left and right eyes of the orbital area.

rent, and exposure time. In a dosimetry study by Kitazato et al. [19] using a water-equivalent material phantom with an ion chamber, the average absorbed dose in the pelvic region was 1.16 ± 0.16 cGy, and 0.23 ± 0.06 cGy in the head region. This is similar to the result obtained in this study, reinforcing its reliability. Under all three scan modes, the highest radiation dose occurred on the surface area and decreased as it moved toward the center. This is consistent with the results obtained for the maximum dose at the surface when the energy was below 400 kV [20].

Assuming a prescribed dose of 1.8 Gy per treatment for the target tumor, as per the cheese phantom experiment results, an additional dose ranging from 0.02% to 0.79% was delivered based on the depth when evaluating the depth dose during a single CBCT scan. In other words, when performing a single CBCT scan, an additional dose is irradiated compared to the prescribed dose. If applied to normal tissues, this poses a risk of additional irradiation owing to CBCT scans, which may increase the likelihood of radiation-induced side effects.

The orbit contains the lens, an important organ in the human body. As radiation therapy progresses, the lens is susceptible to opacification at a threshold dose of 0.5–2 Gy and cataracts at 4 Gy [21–23]. Therefore, we fabricated a human body phantom using a 3D printer and conducted a dose evaluation in the orbit area in this study. Our findings revealed that higher doses near the surface have the most significant impact on the lens. This is similar to the study results by Choi et al. [23] and Kim [24], with a slight difference in the mGy value. Therefore, the results of our study are credible.

During radiation therapy, CBCT scans are performed periodically depending on the frequency and purpose of treatments for patients. Radiation exposure through CBCT is evaluated based on CTDI values. However, the CTDI values only

represent the amounts of X-rays generated from the source. Therefore, it is not the actual dose delivered to the patients [25].

In the study by Park et al. [26], experiments with the Rando phantom yielded an average dose of 22.28 mGy for a single pelvic CBCT scan. Additionally, Amer et al. [27] conducted a study utilizing the Rando phantom to measure CBCT doses. However, differences in the average dose evaluation of the head, chest, and pelvis regions reveal challenges in determining doses according to the location of tumors and critical organs within the human body during radiation therapy.

This study assessed depth-based dosing and evaluated the effect of CBCT on patients using a self-fabricated human body phantom. These study results can be effectively applied to establish an efficient radiation treatment and dose reduction plan by predicting the dose at each location according to the frequency and cycle of CBCT image acquisition.

Conclusion

In this study, we evaluated the radiation dose from CBCT to determine its safety in humans, considering its recent importance in radiation therapy. Results showed an additional dose of 0.02%–0.79% at varying depths compared to the prescribed dose of 1.8 Gy. According to the International Commission on Radiation Units and Measurements (ICRU) 62 recommendation [28], tumor doses from CBCT scans are deemed acceptable if they are at a maximum of 107% or less of the prescribed dose, indicating compliance with recommended standards. Moreover, normal tissue doses during a single CBCT scan varied from 0.39 mGy to 14.14 mGy depending on the location, with an average orbital area dose of 2.15 mGy. However, the value obtained is the dose from a single CBCT scan. Assuming that the frequency of CBCT scans increases as the number of treatments increases, it cannot be dismissed that there is no effect on the human body. Notably, stochastic effects due to CBCT image acquisition cannot be ruled out.

Through this study, it is anticipated that additional doses according to depth variation for each imaging condition can be predicted. By predicting additional doses for key critical organs during the planning stages of therapy, it is expected that adverse effects and complications resulting from radiation therapy can be minimized.

Therefore, radiation workers should consider the radiation exposure dose based on the number of CBCT retakes, imag-

ing scan modes, and imaging scan cycles and should strive to keep the radiation exposure dose to patients as low as possible according to the as low as reasonably achievable principle.

Conflict of Interest

No potential conflict of interest relevant to this article was reported.

Ethical Statement

This article does not contain any studies with human participants or animals performed by any of the authors.

Author Contribution

Conceptualization: Lee DY. Methodology: Kang YR. Formal analysis: Kim HJ. Project administration: Lee DY. Writing - original draft: Choi MH. Writing - review & editing: all authors. Approval of final manuscript: all authors.

References

- Kim DY, Park SY. Proton beam therapy. *J Korean Med Assoc.* 2008;51(7):638–642.
- Ling CC, Burman C, Chui CS, Kutcher GJ, Leibel SA, LoSasso T, et al. Conformal radiation treatment of prostate cancer using inversely-planned intensity-modulated photon beams produced with dynamic multileaf collimation. *Int J Radiat Oncol Biol Phys.* 1996;35(4):721–730.
- Bortfeld T, Boyer AL, Schlegel W, Kahler DL, Waldron TJ. Realization and verification of three-dimensional conformal radiotherapy with modulated fields. *Int J Radiat Oncol Biol Phys.* 1994; 30(4):899–908.
- Chui CS, LoSasso T, Spirou S. Dose calculation for photon beams with intensity modulation generated by dynamic jaw or multileaf collimations. *Med Phys.* 1994;21(8):1237–1244.
- Meijer GJ, Rasch C, Remeijer P, Lebesque JV. Three-dimensional analysis of delineation errors, setup errors, and organ motion during radiotherapy of bladder cancer. *Int J Radiat Oncol Biol Phys.* 2003;55(5):1277–1287.
- Bak J, Jeong K, Keum KC, Park SW. On-line image guided radiation therapy using cone-beam CT (CBCT). *J Korean Soc Ther Radiol Oncol.* 2006;24(4):294–299.
- Oh S, Kim S, Suh TS. How image quality affects determination of target displacement when using kilovoltage cone-beam computed tomography. *J Appl Clin Med Phys.* 2006;8(1):101–107.
- Song JY, Nah BS, Chung WK, Ahn SJ, Nam TK, Yoon MS. Analysis of respiratory motional effect on the cone-beam CT image. *Korean J Med Phys.* 2007;18(2):81–86.
- Murphy MJ, Balter J, Balter S, BenComo JA Jr, Das IJ, Jiang SB, et al. The management of imaging dose during image-guided radiotherapy: report of the AAPM Task Group 75. *Med Phys.* 2007; 34(10):4041–4163.
- Létourneau D, Wong JW, Oldham M, Gulam M, Watt L, Jaffray DA, et al. Cone-beam-CT guided radiation therapy: technical implementation. *Radiother Oncol.* 2005;75(3):279–286.
- Khan M, Sandhu N, Naeem M, Ealden R, Pearson M, Ali A, et al. Implementation of a comprehensive set of optimised CBCT protocols and validation through imaging quality and dose audit. *Br J Radiol.* 2022;95(1139):20220070.
- Lee SU. Evaluation of DQA for tomotherapy SRS using 3D volumetric phantom [master's thesis]. Department of Radiological Science, The Graduate School of Hanseo University; 2016.
- Yadav P, Tolakanahalli R, Rong Y, Paliwal BR. The effect and stability of MVCT images on adaptive tomotherapy. *J Appl Clin Med Phys.* 2010;11(4):3229.
- Allsabbagh M, Tajuddin AA, Manap MA, Zainon R. Evaluation of nine 3D printing materials as tissue equivalent materials in terms of mass attenuation coefficient and mass density. *Int J Adv Appl Sci.* 2017;4(9):168–173.
- Araki F, Ikegami T, Ishidoya T, Kubo HD. Measurements of gamma-knife helmet output factors using a radiophotoluminescent glass rod dosimeter and a diode detector. *Med Phys.* 2003;30(8): 1976–1981.
- Rah JE, Shin DO, Hong JY, Kim HS, Lim CI, Jeong HG, et al. Study on dosimetric properties of radiophotoluminescent glass rod detector. *J Radiat Prot.* 2006;31(4):181–186.
- Son SJ, Park JK, Jung DK, Park MH. Comparison of the equivalent dose of the lens part and the effective dose of the chest in the PET/CT radiation workers in the Nuclear Medicine Department. *J Radiol Sci Technol.* 2019;42(3):209–215.
- International Atomic Energy Agency. Radiation protection and safety of radiation sources: international basic safety standards. General Safety Requirements Part 3. IAEA; 2014.
- Kitazato Y, Kuga N, Shirieda K, Enzaki M, Nakaguchi Y, Shimohigashi Y, et al. Evaluation of absorbed dose for CBCT in image-guided radiation therapy: comparison of each devices and facilities. *Nihon Hoshasen Gijutsu Gakkai Zasshi.* 2017;73(4):309–316 (Japanese).
- Khan FM. *The physics of radiation therapy.* 4th ed. Lippincott Williams & Wilkins; 2010.
- Hall EJ, Giaccia AJ. *Radiobiology for the radiologist.* 6th ed. Lippincott Williams & Wilkins; 2006. p. 181–186.
- Pawlicki T, Luxton G, Le QT, Findley D, Ma CM. Lens dose in MLC-based IMRT treatments of the head and neck. *Int J Radiat Oncol Biol Phys.* 2004;59(1):293–299.

23. Choi JW, Kim CC, Park SY, Song KW. Evaluation of the lens absorbed dose of MVCT and kV-CBCT use for IMRT to the nasopharyngeal cancer patient. *J Korean Soc Radiat Ther.* 2013;25(2): 131–136.
24. Kim JB. Characteristics and absorbed dose analysis of CBCT for radiation therapy [master's thesis]. Department of Radiological Science, Graduate School, Catholic University of Pusan; 2018.
25. Moon YM. A study on the effective dose measurement for cone beam computed tomography using glass dosimeter [master's thesis]. Department of Physics, Graduate School of Dong-A University; 2013.
26. Park BS. Analysis of dose distribution versus patient exposed dose according to the frequency of cone beam computerized tomography for prostate intensity modulated radiation therapy [master's thesis]. Department of Medical Physics, The Graduate School of Bio-Medical Science Korea University; 2014.
27. Amer A, Marchant T, Sykes J, Czajka J, Moore C. Imaging doses from the Elekta synergy X-ray cone beam CT system. *Br J Radiol.* 2007;80(954):476–482.
28. International Commission on Radiation Units and Measurements. ICRU Report 62: Prescribing, recording and reporting photon beam therapy (Supplement to ICRU report 50). *J ICRU.* 1999; 32(1):1–52.